ADVANCED FUNCTIONAL MATERIALS
www.afm-journal.de

Photo-Arbuzov Reactions as a Broadly Applicable Surface Modification Strategy

*Martina Plank, Anthony Berardi, Alexander Welle, Eric Sauter, Peter Krolla, Cristian Haret, Meike Koenig, Mareen Stahlberger, Zahid Hassan, Simon Oßwald, Stefan Bräse, and Joerg Lahann**

Chemical vapor deposition (CVD) polymerization is a commonly used approach in surface chemistry, providing a substrate-independent platform for bioactive surface functionalization strategies. This work investigates the Arbuzov reaction of halogenated polymer coatings readily available via CVD polymerization, using poly(4-chloro-*para*-xylylene) (Parylene C) as a model substance. Postpolymerization modification of these coatings via catalyst-free and UV-induced Arbuzov reaction using phosphites results in phosphonate-functionalized polymers. The combination of infrared reflection-absorption spectroscopy (IRRAS), X-ray photoelectron spectroscopy (XPS), and time-of-flight secondary ion mass spectrometry (ToF-SIMS) provides detailed insights into the reaction progress. Time-dependent studies suggest that the non-polar phosphites penetrate deep into the CVD films and react with the polymer film. In addition, ToF-SIMS, scanning electron microscopy (SEM), and atomic force microscopy (AFM) confirm spatial control of the reaction, resulting in localized chemical and topographical surface modification, recognizable by changes in interference color, fluorescence, and wettability. Preliminary 3D fluorescence spectroscopy investigations indicate tunable near-infrared emission of these polymer films. This work is the first step toward generating multifunctional polymer coatings based on chemically modifiable, CVD polymers with potential applications in biomaterials, sensors, or optoelectronics.

1. Introduction

Poly(*para*-xylylenes) (PPX), also known under the trade name "Parylene," are industrially used coatings obtained by chemical vapor deposition (CVD) polymerization using a variety of [2.2]paracyclophanes (PCP). This type of polymer was first discovered in 1947 by Szwarc, who observed the formation of PPX after the pyrolysis of *para*-xylylene.[1,2] To date, the most common polymerization is based on the Gorham process, first described in 1966, which uses volatile PCP precursor molecules.[3,4] This three-step process is carried out under vacuum (0.1–0.3 mbar) and involves sublimation of PCP (100–200 °C) followed by pyrolysis to generate 1,4-quinodimethane radicals (550–800 °C), and deposition of the radicals (<30 °C), resulting in conformal polymer films (**Figure 1**). Nonfunctional and halogen-bearing PCPs are readily available and can serve as commercial precursors for barrier coatings such as Parylene N, C, D, HT, and AF-4, which feature high solvent, temperature,

M. Plank, A. Welle, E. Sauter, P. Krolla, C. Haret, M. Koenig, J. Lahann
Institute of Functional Interfaces (IFG)
Karlsruhe Institute of Technology (KIT)
76131 Karlsruhe, Germany
E-mail: lahann@umich.edu

The ORCID identification number(s) for the author(s) of this article can be found under https://doi.org/10.1002/adfm.202403408

DOI: 10.1002/adfm.202403408

M. Plank, S. Bräse, J. Lahann
Soft Matter Synthesis Laboratory
Institute for Biological Interfaces 3 (IBG-3)
Karlsruhe Institute of Technology
76131 Karlsruhe, Germany

A. Berardi, J. Lahann
Biointerfaces Institute
Macromolecular Science and Engineering Program
University of Michigan
Ann Arbor, MI 48109, USA

M. Stahlberger, Z. Hassan, S. Oßwald, S. Bräse
Institute of Organic Chemistry (IOC)
Karlsruhe Institute of Technology
76131 Karlsruhe, Germany

S. Bräse
Institute of Biological and Chemical Systems - Functional Molecular Systems (IBCSFMS)
Karlsruhe Institute of Technology
76131 Karlsruhe, Germany

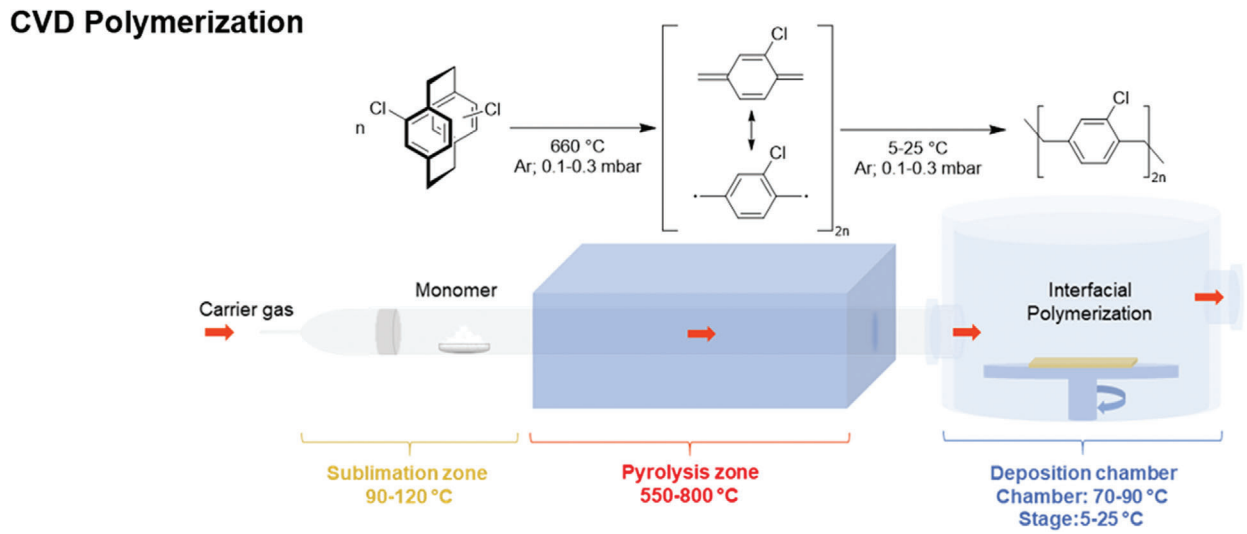

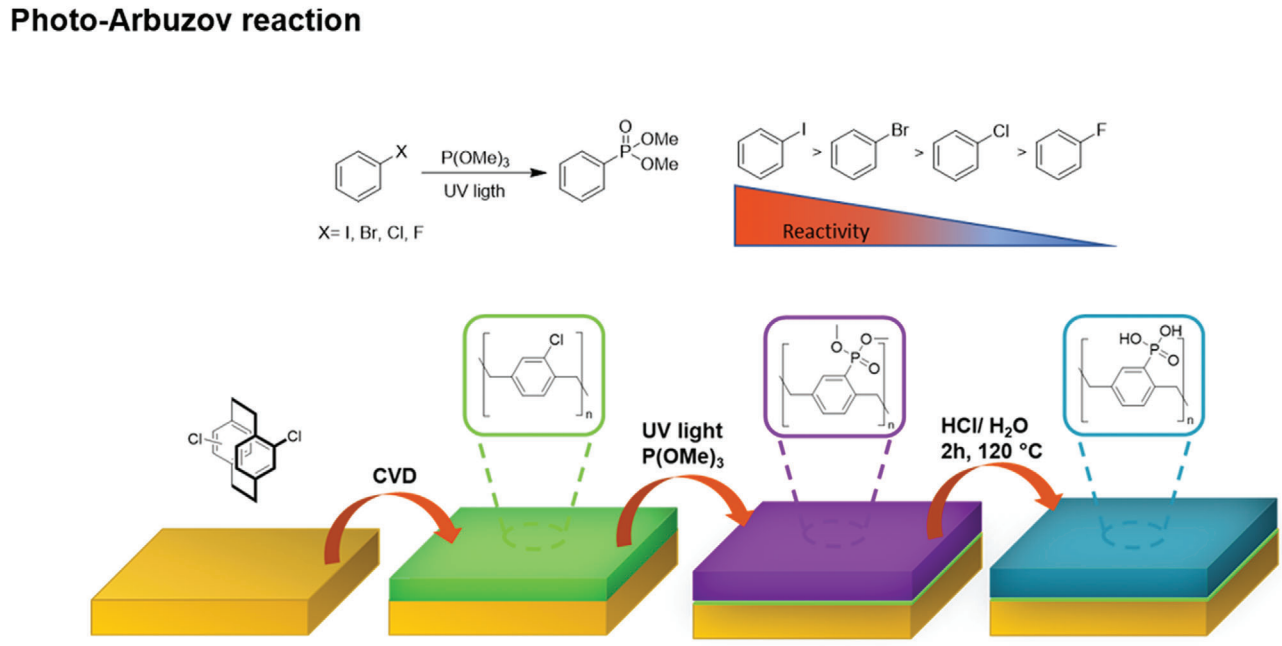

Figure 1. Concept and reaction scheme of CVD polymerization forming poly(*para*-xylylene) thin films (top). Schematic depiction of surface modification steps from hydrophobic surface originated by Parylene C deposition to the hydrophilic surface by phosphorylation using UV-catalyzed Arbuzov reaction (bottom).

and chemical stability with low dielectric constants.[5–7] Based on this solvent-free, quantitative, and clean polymerization process, pinhole-free PPX layers are accessible, which are essential for a wide range of high-tech applications, such as electronics,[8–10] medical devices,[11–13] sensors,[14] microelectromechanical systems (MEMS),[15–17] photovoltaic[18] and microfluidics.[19,20] Due to a growing demand for reactive and bioactive coatings, CVD polymerization of different functional PCP monomers has been pursued to prepare multifunctional and structured surfaces with significant potential in biomaterials.[6,21,22] Furthermore, recent research has focused on 3D structures templated by materials like ice,[23,24] electrospun polymer sponges,[25] liquid crystals (LC),[26,27] or metal-organic frameworks (MOF).[28] These approaches offer a combination of nano-/micro-/mesoscale structures with remarkable functionality and stability, rendering them ideal for diverse research areas. Although various functional PCP precursors are known in the literature, only a few polar PPX coatings (Parylene A/AM and HT) are commercially available.[6,22,29]

In addition to altering the functionality by copolymerizing vinyl monomers,[6,30] various methods have been used to modify the surface properties of commercial Parylene C and N. A

popular method is non-specific treatment with oxygen plasma, which improves surface wettability by introducing polar groups and modulates the surface roughness, leading to improved cell adhesion and proliferation while preserving the original mechanical properties of the PPX layer.[31–34] Furthermore, "click" chemistry in combination with the substrate-independent CVD polymerization has been used as a platform technology for bioactive surface functionalization.[22,35] For example, alkyne and pentafluorophenyl ester functionalities have been introduced to PCP monomers to enable alkyne-azide cycloaddition and active ester-amine reactions on the resulting PPX surfaces, allowing for co-presentation of cyclic arginine-glycine-aspartic acid (cRGD) adhesion peptide and epidermal growth factor (EGF), respectively.[36] The combination of alkyne with reactive double bonds, aldehyde, or amine functional groups has also proven to be an effective strategy for the orthogonal binding of biomolecules, fluorophores, or polymers.[37–39] Alternatively, direct functionalization of non-reactive Parylene coatings via chemical reactions such as sulfonation,[40] Friedel-Crafts reactions,[40,41] aminomethylation,[40] and Buchwald-Hartwig amination has been reported.[42] Although most of these reactions are efficient, catalysts, organic solvents, and high-temperature conditions are generally required. An alternative postpolymerization modification method involved photoinduced, phospholipid polymer grafting with benzophenone as the photoinitiator.[43] Approaches to surface functionalization commonly utilize nature as a model and often involve grafting biomolecules[44] like peptides,[41] proteins,[45] amino acids,[46] and phospholipids.[43]

Here, we report novel phosphorus-containing surfaces, such as phosphates and phosphonates, that are essential components in biological systems and exhibit interesting electronic properties due to their free d-orbitals that interact and form bonds with (metal)ions or provide superior conductivity.[47,48] The choice of the phosphorus motif depends on the desired application, with the stability of the compound being the most important design criterion. Phosphorus-containing motifs are highly relevant to the fields of osteogenic differentiation,[49,50] (bio)sensors,[51,52] and membrane technology,[48,53,54] as well as flame retardant,[55] anti-corrosive[56] and anti-fouling[57] films. Aliphatic phosphate and phosphonate polymers containing ester and amide functionalities, which show lower stability against hydrolysis and degradation, were widely used in biomedical applications due to their ability to degrade under physiological conditions.[58] In contrast, phosphorus-containing aromatic polymers are highly stable in corrosive and/or oxidative environments and higher temperatures.[47] More recently, biointerfaces with phosphorous-containing polymers have been explored for applications in antimicrobial and antifouling surfaces, lubrication, mineralization, and bone targeting.[59,60]

This work introduces a novel class of phosphonated Parylene surfaces generated by postpolymerization modification of commercially available Parylene C films. This transformation utilized the UV-induced photo-Arbuzov reaction, which was first published in 1966 by Griffin and co-workers[61,62] and was reinvestigated by Oßwald et al. in 2022.[63] Herein, aromatic systems bearing halogens are transformed into various phosphonates with UV light in the absence of a catalyst which is advantageous over other UV-induced transformations that require photo-redox or base catalysts.[64–67] Building upon this emergent body of work, we developed a general approach to phosphorus-containing surfaces with tailored functionality based on CVD polymerization and subsequent post-polymerization modification with phosphites.

2. Results and Discussion

Phosphonated PPX films were fabricated in a two-step process using CVD polymerization first to generate a conformal Parylene C coating, followed by a polymer analogous conversion utilizing the UV-catalyzed photo-Arbuzov reaction, as illustrated in Figure 1. As a last step, acid-catalyzed hydrolysis led to the formation of surface coatings decorated with phosphonic acid groups. This work used Parylene C as a model substrate for its industrial relevance. This reaction is applied to a wide range of halogen-containing aromatic systems.[61,63,64] For these systems, the halide's reactivity is determined by the bond dissociation energy (BDE) of the aryl derivatives (BDE: C—I < C—Br < C—Cl < C—F) and the polarity of the reactants.[68–70] An excess of phosphite was required to ensure the complete conversion of aryl halides, which was reasonable given the reaction mechanism through an electron donor-acceptor (EDA) complex formation.[62,71] This UV-catalyzed photo-Arbuzov reaction was activated by the formation of a non-covalent halogen-bond complex (HB) that exhibits an attractive interaction between an electron-acceptor molecule, the aryl halide, and an electron-donor molecule, the phosphite, characterized by a partial $n \rightarrow \sigma^*$ charge transfer. Upon irradiation, a highly reactive aryl radical was formed due to photo-induced electron transfer (PET), which subsequently reacted with a phosphite and rearranged to form the phosphonate.[71]

According to the BDE of aryl halides, the bond scission of aryl iodides and bromides can be activated by visible light, while higher energy is required for aryl chlorides and fluorides. In this work, the universal UV-catalyzed photo-Arbuzov reaction of Parylene C polymer films with phosphites was investigated in a time-dependent manner using ellipsometry, infrared reflection-absorption spectroscopy (IRRAS), and X-ray photoelectron spectroscopy (XPS) (see **Figure 2**). In this experiment, $P(OMe)_3$ was chosen as a model phosphite. In addition, the applicability to bromides and fluorides containing precursor polymers was also demonstrated (Figure S1, Supporting Information). In general, the reaction started immediately upon irradiation with UV-light at 251 nm. After 0.5 h, significant polymer transformations were observed with various analytical methods. Ellipsometry measurements based on a multiwavelength Cauchy model (Figure S2, Supporting Information) showed an increase in film thickness and a decrease in refractive index (Figure 2A). After 2 h, the film thickness and refractive index plateaued, with an increase in film thickness of 22.7 nm relative to the original Parylene C film (54.9 nm), while the refractive index at 632 nm decreased from 1.62 to 1.55. Following this plateau, a significant change was observed after 6 h, attributable to side reactions, such as oxidative decomposition.[72] After 6 h reaction time, the XPS spectrum displayed an additional oxygen signal (Figure 2C, O 1 s signal).[73] Additional measurements up to a reaction time of 24 h are shown in the supporting information (Table S1 and Figure S3, Supporting Information). IRRAS investigation showed an increase in phosphonate-specific bands at 1254, 1000–1100, and 829 cm^{-1}, reaching a nearly constant intensity after 2 h.

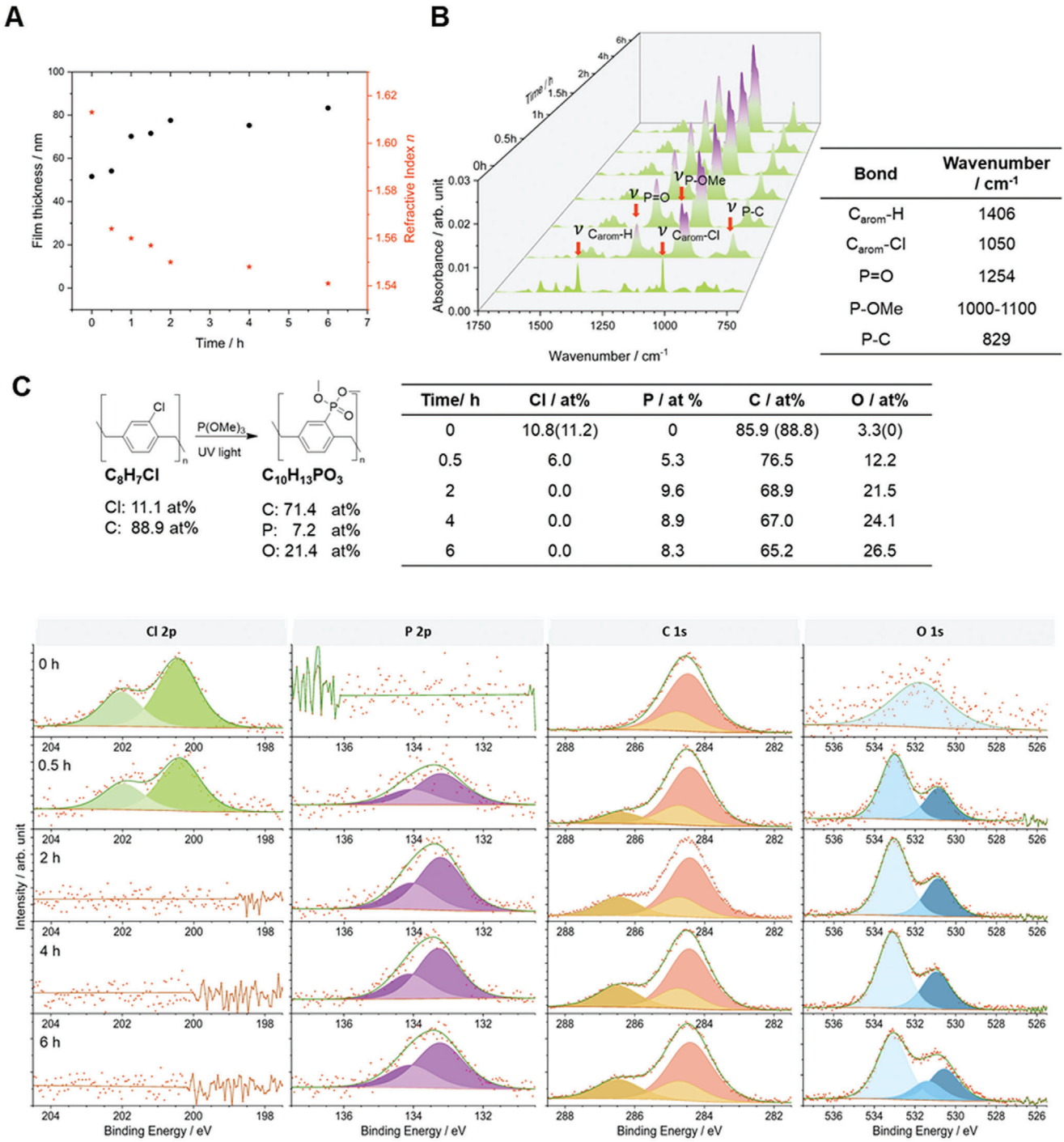

Bond	Wavenumber / cm^{-1}
C_{arom}-H	1406
C_{arom}-Cl	1050
P=O	1254
P-OMe	1000-1100
P-C	829

Time/ h	Cl / at%	P / at %	C / at%	O / at%
0	10.8(11.2)	0	85.9 (88.8)	3.3(0)
0.5	6.0	5.3	76.5	12.2
2	0.0	9.6	68.9	21.5
4	0.0	8.9	67.0	24.1
6	0.0	8.3	65.2	26.5

Figure 2. Time-dependent conversion of Parylene C to Parylene PO(OMe)$_2$ by photo-Arbuzov reaction monitored by A) ellipsometry, B) IRRAS, and C) XPS.

Concurrent with the increase in phosphonate bands was a decrease in the sharp band at 1406 cm^{-1} corresponding to the characteristic C—H vibration of the monosubstituted aromatic ring of Parylene C (Figure 2B). Quantitative information about the film composition was obtained from XPS measurements shown in Figure 2C. The transformation, which is consistent with pseudo-first order reaction kinetics,[74,75] was completed after 2 h as indicated by the absence of the chlorine signal and the constant ratio of the phosphorus signal.

Moreover, the composition of the film with 9.6 at% phosphorus, 68.9 at% carbon, and 21.5 at% oxygen corresponded closely to the theoretically calculated composition (7.2 at% phosphorus, 71.4 at% carbon, and 21.4 at% oxygen). The observed deviations were within the range of the method's error. The composition of

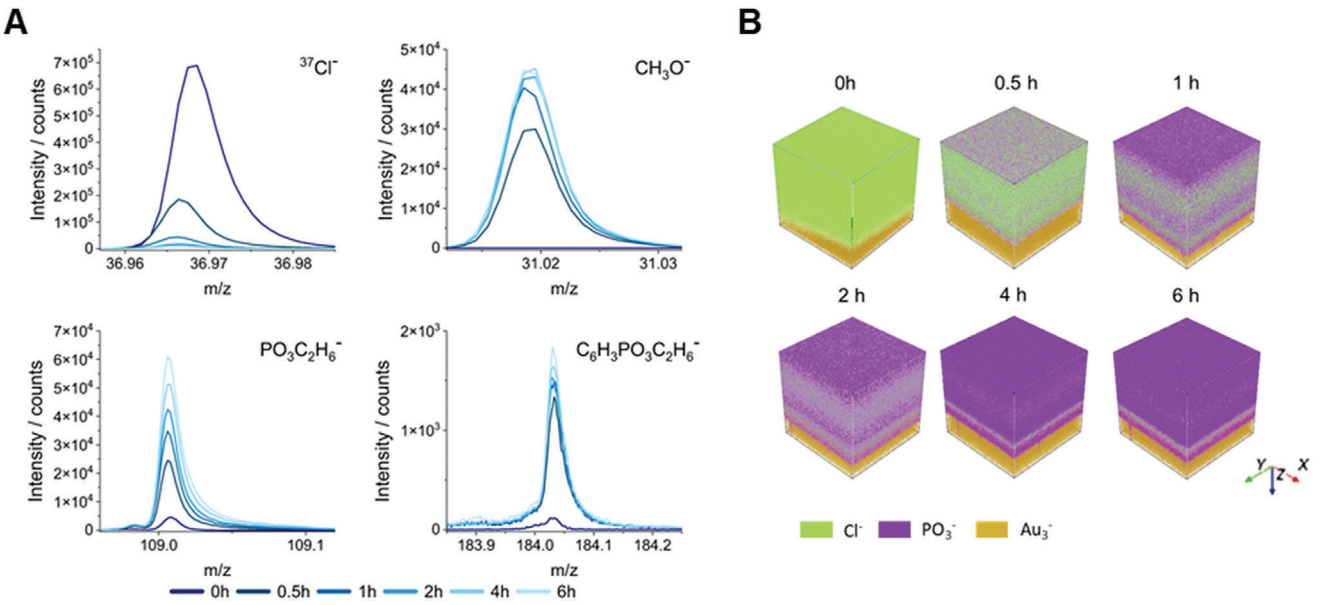

Figure 3. A) ToF-SIMS analysis of the UV-treated surfaces after 0, 0.5, 1, 2, 4, and 6 h, represented by the characteristic fragments $^{37}Cl^-$, CH_3O^-, $PO_3C_2H_6^-$ and $C_6H_3PO_3C_2H_6^-$ indicating the progress of the photo-Arbuzov reaction. B) The 3D representation of the measured Cl^- and PO_3^- ions using ToF-SIMS depth profiling (*x* and *y* 500 µm, *z* not to scale).

the original Parylene C film also matched the theoretical values, i.e., 11.1 at% chlorine and 88.9 at% carbon. In addition, a small amount of oxygen (3.3 at%) was detected, attributed to slight impurities on the film's surface or radical quenching by oxygen during polymerization. The methods confirmed a rapid and quantitative reaction of the PPX-Cl to the product, PPX-$PO(OMe)_2$. As a control experiment, unfunctionalized Parylene N was treated with phosphite. This experiment was designed to rule out the formation of phosphonates due to the formation of radicals induced by UV-light. After 6 h of irradiation, the Parylene N coating showed no significant change in film thickness and IR spectrum (Figure S4 and Table S2, Supporting Information), confirming the selective nature of the photo-Arbuzov reaction of $PO(OMe)_2$ with Parylene C.

Since Parylene coatings are described in the literature as chemically inert, dense barrier layers, the progression of the reaction into the bulk of the polymer films was unexpected.[12,13,43] We sought to determine whether the reaction proceeds stepwise or homogenously throughout the layer and performed time-of-flight secondary ion mass spectrometry (ToF-SIMS) studies to gain further insight (**Figure 3**). First, surface measurements were conducted using Bi_3^+ clusters for soft matter sputtering and ionization. Using negative analyzer polarity, we were able to detect specific fragments for all reactants. Figure 3A shows the progression of the reaction over time based on the evolution of the $^{37}Cl^-$ signal, which is indicative of the starting material, Parylene C, and the OCH_3^- and $PO_3C_2H_6^-$ signals arising from the newly formed phosphonate groups. In addition, the emergence of the $C_6H_3PO_3C_2H_6^-$ fragment was detected over time, confirming the transformation of the chlorine into phosphonate groups. Overall, the ToF-SIMS investigation of the surface supported the findings previously obtained by XPS and IRRAS measurements, as the absence of chlorine ions and the saturation of phosphonate-specific fragments indicated almost complete conversion after 2 h of irradiation.

Additional depth profiles were measured to evaluate inhomogeneities within the polymer films. Argon clusters were used for depth profiling followed by ToF-SIMS analysis using Bi_3^+ clusters in the negative analyzer mode. This approach allowed for stepwise analysis of the polymer film with increments of a few nanometers until the gold substrate was reached. Because ToF-SIMS measurements have an excellent depth resolution of about 6 nm, it was possible to gain a detailed insight into vertical changes in the composition of the polymer films. Figure 3B shows the 3D distribution of the specific ions through the film and demonstrates the depth profiles of 500 × 500 µm^2 regions of the Parylene C films after defined irradiation times. These depth profiles suggest that the phosphite penetrates the Parylene C layer. It also confirmed that the reaction occurred throughout the bulk of the polymer film. After 4 h, an almost complete conversion was reached. The reaction progresses very fast as extensive surface modification was achieved after only 1 h (Figure 3B). A closer look at the depth profiles after 4 h and 6 h revealed a distinct chlorine-containing layer at the polymer–gold interface, which is probably responsible for the adhesion of the film to the surface after 6 h. After 8 h, the film started to delaminate, indicating the complete conversion of the remaining chlorinated layer. The delamination reflected the nonadhesive properties of phosphonated Parylene polymer due to repulsive forces. When polymerizing monofunctionalized PCP-$PO(OMe)_2$ via CVD polymerization, we observed a polymer coating that exhibits poor adhesion to gold, silicon, and aluminum surfaces (Table S3 and Figure S5, Supporting Information). The reported synthetic strategy opens the door to various applications of phosphonate-containing PPX films with high interfacial adhesion. Due to PCP-Cl's ability to readily polymerize via CVD polymerization, phosphonate

surfaces with good adhesion or surface-independent free-standing films can be prepared straightforwardly.[74,75]

The hydrolysis of phosphonic acid dimethyl ester was further investigated as a polymer-analogue surface modification approach. Three strategies were described in the literature to hydrolyze phosphonate diesters: alkaline hydrolysis and hydrolysis by Lewis or mineral acids.[76,77] The preferred method in industry and laboratories is the use of trimethylsilyl (TMS) halides, but due to disadvantages such as high price, toxicity, and moisture sensitivity, the use of acids is commonly considered as an alternative, especially in biomedical research. Although hydrobromic acid (HBr) is more effective, hydrochloric acid (HCl) is preferred for safety reasons because HBr can generate alkyl bromides during hydrolysis.[76] In addition, *p*-toluenesulfonic acid (*p*-TsOH) was also used as a less corrosive acid in addition to HCl, so the hydrolysis of PPX-$PO(OMe)_2$ to $PO(OH)_2$ with both acids was examined under different conditions (Figure S6, Supporting Information). The best results were achieved by treating the surface with HCl (6 M) for 2 h at 120 °C. IRRAS, XPS, and ToF-SIMS measurements confirmed the hydrolysis of free phosphonic acid. The XPS and ToF-SIMS results still showed residual signals corresponding to methoxy groups from $PO(OMe)_2$ (**Figure 4**). The XPS analysis showed a conversion of 88.3%, estimated from the methoxy carbon C 1s signal at 286.5 eV. This value might be underestimated, as even the XPS analysis did not reveal any detectable signal of O 1s at around 533.1 eV corresponding to the binding energy of P—O—CH_3. Due to the limitation of the XPS setup and the comparable high full-width half maximum (FHWM), the signal corresponding to the C 1s of the O—CH_3 group might be overestimated. Contact angle measurements complemented IRRAS, XPS, and ToF-SIMS measurements to illustrate the hydrophilicity induced during the transformation (Figure 4D). The water contact angles of the functional surfaces were as expected in the order PPX-Cl > PPX-$PO(OMe)_2$ > PPX-$PO(OH)_2$, with 95° > 57° > 49°, respectively. Moreover, different contact angles were measured for both phosphonated PPX films depending on the degree of dryness (Table S4, Supporting Information), indicating different hydration states of the surfaces, which will be further investigated in future work.

Photocatalyzed reactions have been widely employed in research and industry due to their excellent spatial and temporal control.[78,79] Since the aryl halide is activated in the presence of a phosphite by exciting the formed EDA complex with UV-light to form a highly reactive aryl radical, high spatial control can be expected.[71,79] Here, transmission electron microscopy (TEM) meshes with different mesh sizes served as a photomask and were attached to the Parylene C surface (**Figure 5**). Phosphite was applied to the surface, and the samples were irradiated in a UV-reactor with radially aligned line sources for 0.5, 2, and 4 h (Figure S7, Supporting Information). The quality of the lithography process was evaluated by SEM, atomic force microscopy (AFM), and ToF-SIMS measurements for samples treated for 4 h (Figure 5B–D). Overall, the structure of the TEM meshes was transferred with high fidelity, as evidenced by the SEM images (Figure 5B). Distinct microstructures of 200 and 60 µm were successfully generated via the lithography process.

Furthermore, the change in topography was confirmed by AFM measurements. The maximum height difference measured with AFM (24.6 nm) agrees with the film thickness increase of 22.7 nm obtained by ellipsometry. It is interesting to note that there was only a small increase in surface roughness during the transformation steps from PPX-Cl to PPX-$PO(OMe)_2$ and to PPX-$PO(OH)_2$, with average roughness R_a values of 1.2, 2.0, and 2.3 nm, respectively. After surface treatment, the PPX-Cl areas increased in R_a to 1.6 nm, indicating that the coating quality was not significantly altered. In addition, a spatially sharply defined chemical transformation was detected throughout the film by ToF-SIMS, as shown in Figure 5B. Interestingly, no blurring of the structure with an increasing penetration depth was observed, making this reaction system suitable for even smaller pattern dimensions than the ones employed in this study.

We demonstrated the modularity of this approach through the variation of the following three variables: choice of halide-containing precursor polymer, composition of the precursor polymer, and sample irradiation time. The system is readily compatible with photolithography, but alternative photopatterning methods such as direct laser writing or photomasking may also be employed. We sought to demonstrate the versatility of the reaction system by using phosphites with different functionalities. Standard analytical techniques, such as ellipsometry and IRRAS, confirmed successful reactions with various phosphites (Table S5 and Figure S8, Supporting Information). In the following section, the polarity and steric effects of various phosphites on the reaction and the resulting properties of the polymers obtained were investigated. Parylene C-coated surfaces were treated with different phosphites under UV-light. The reaction progress was investigated by ToF-SIMS depth measurements after 2 h, shown in **Figure 6** showing CVD-based polymer films modified by photo-Abuzov rection with selected phosphites. The detailed distributions of the characteristic fragments can be found in Figures S9 and S10 (Supporting Information). First, it was found that non-polar reactants such as phosphites with hydrocarbons (methyl-, isopropyl-) or the trifluorethyl derivative showed homogeneous reaction with Parylene C throughout the film. In contrast, the more polar tris-(trimethylsiliyl)-phosphite ($P(OSi(CH_3)_3)_3$) reacted only with the surface of the film. In addition, reactions of various phosphites with hydrocarbons that have high steric effects and thus a large positive inductive (+I) or mesomeric (+M) effect (hydrocarbons: neopentyl-, benzyl-, phenyl-) showed no appreciable conversion to the corresponding phosphonate polymers, represented by $P(OC_6H_5)_3$ in Figure 6. This was accompanied by a color change of the surrounding phosphite solution from transparent to brownish, indicating instability of the phosphites under UV-irradiation and ambient conditions. It should be mentioned that the reaction with $P(OSi(CH_3)_3)_3$ and $P(OCH(CF_3)_2)_3$ was terminated after 30 and 60 min , respectively. The different characteristics of the phosphites resulted in various phosphonated surfaces with distinct surface wettability, as confirmed by water contact angle (WCA) measurements and characteristic fluorescence shown in Figure 6. 3D excitation-emission spectra showed a trend of increasing intensity of emission ($P(OCH_3)_3$ < $P(OCH(CH_3)_2)_3$ < $P(OSi(CH_3)_3)_3$) and a shift to longer wavelengths, which can be explained by the electron-donating properties of the substituent bound to phosphorus.[80] Silyl trimethyl groups, which represent the strongest electron-donating substituent in this work due to free ion pairs inducing a +M-effect, stabilize the excited

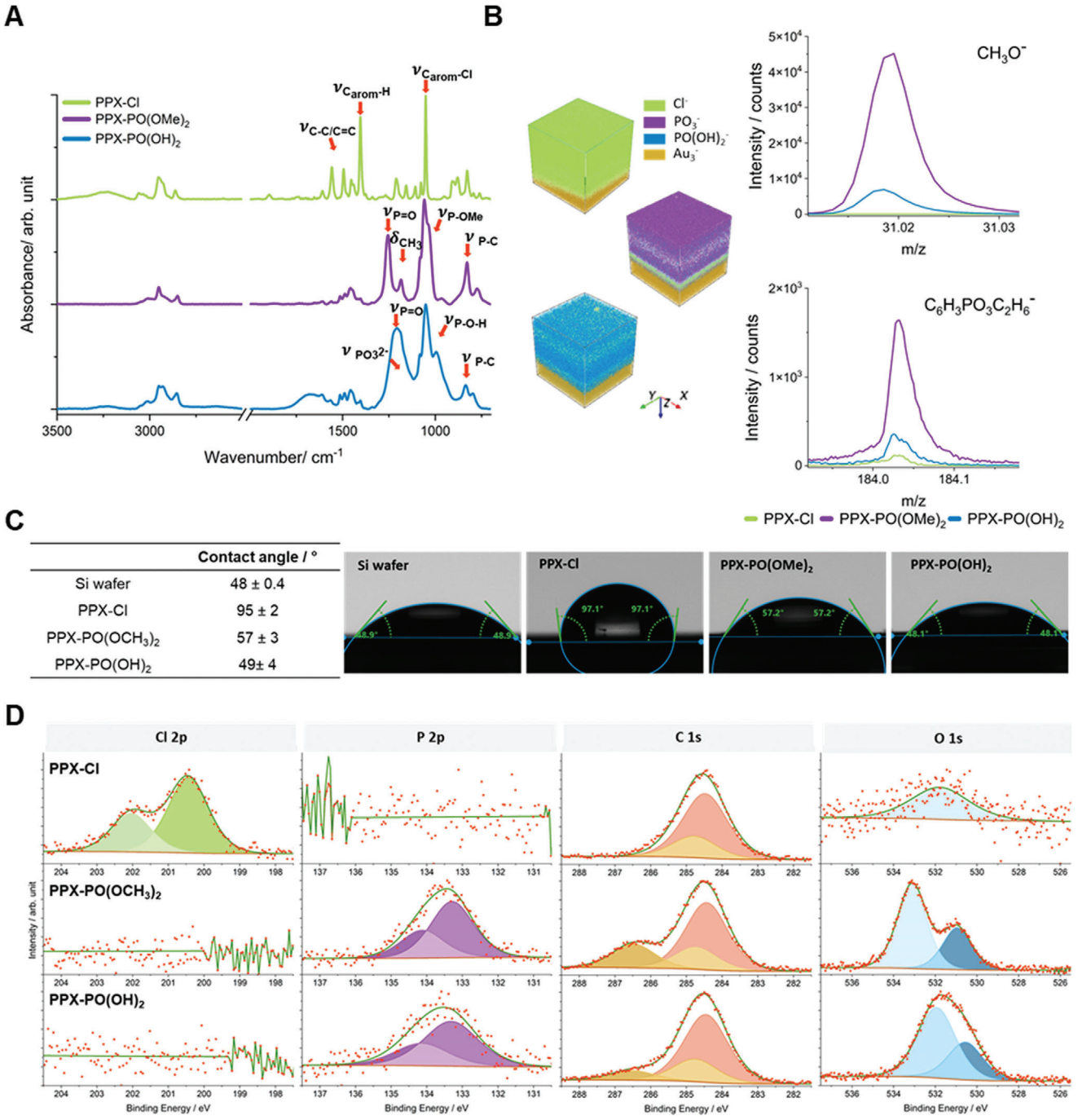

Figure 4. Transformation from hydrophobic Parylene C to hydrophilic PCP-PO(OH)$_2$ investigated by IRRAS with assignments according to literature.[80–82] A) ToF-SIMS depth profile, and surface measurements (x and y 500 µm, z not to scale) B) as well as XPS data. The change of surface polarity is visualized by the illustration of one exemplary contact angle measurement and the mean value from N = 10 measurements with the corresponding standard deviation.

state (π^*). Such stabilized electronic systems led to a broader emission spectrum and were excited at red-shifted wavelengths (up to 400 nm) compared to PPX-PO(OCH$_3$)$_2$. An even larger red shift was observed for fluorine-containing substituents, which have a high electron-withdrawing nature and relatively high-energy orbitals, influencing the energy level of the molecular orbitals.[80] In addition, introducing fluorine atoms generally lead to increased conjugation and thus to an expansion of the delocalized system, resulting in red-shifted emission.

Rigid phosphonated materials have recently gained attention due to their fluorescent properties as emitters in the UV–vis and near-infrared (NIR) regions. Similar effects can be observed in

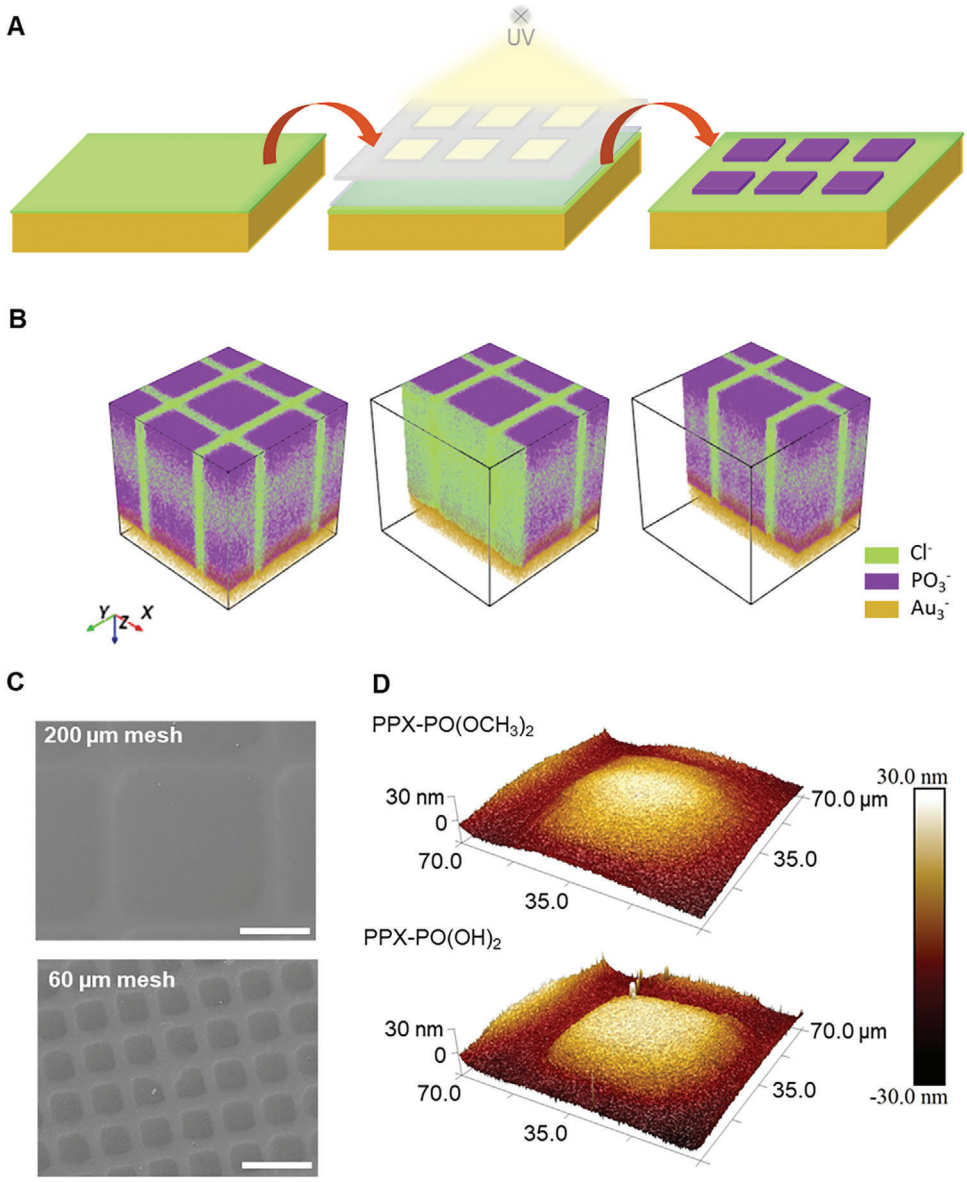

Figure 5. A) Site-selective conversion of Parylene C to the phosphonated PPX polymer using TEM grids as photomasks illustrated. B) The quality in spatial control was investigated by ToF-SIMS in-depth measurements showing Parylene C in green (Cl^-) and phosphonated PPX in purple (PO_3^-) (*x* and *y* 500 µm, *z* not to scale). C) Furthermore, the accuracy of the structure transfer by using TEM grids with a size of 60 µm and 200 µm is shown by SEM measurements displaying top-views of PPX-$PO(OH)_2$ films with a scale bar of 100 µm. AFM measurements of patterned films (60 µm TEM grid) D) after conversion to the phosphonate (top) and cleavage to the free phosphonic acid (bottom), illustrating the topographical effect of the treatments and confirming a 24.6 nm height increase.

the phosphonated thin films presented in Figure 6 and Figures S11–S13 (Supporting Information).[81] Moreover, room temperature phosphorescence (RTP) of phosphonate systems has been reported in few instances.[82–84] In this work, phosphorescence was not detectable. However, the absorption spectra showed evidence for intersystem crossing (ISC) from the singlet S_1 to the triplet T_1 state, which can be enhanced by intelligent material design, e.g., by doping with (metal) ion or the introduction of polar counterparts that might result in an afterglow system. Materials with this optoelectronic property have potential applications in information encryption, anti-counterfeiting, optoelectronics like light-emitting diodes, medical diagnostics and biomedical imaging, and sensing.[85-89]

Next, thicker Parylene C films (>200 nm) and free-standing polymer films were evaluated, as properties often change with increasing thickness of the polymer system. The photo-Arbuzov reaction for thicker layers was directly visible by fluorescence upon excitation with UV-light using 254 and 365 nm wavelengths, respectively (see **Figure 7**). In addition, Figure 7B demonstrates spatial controllable reaction using a photomask, achieving localized color change, wettability, and fluorescence of Parylene C-coated silicon surfaces. Furthermore, the investigation of the

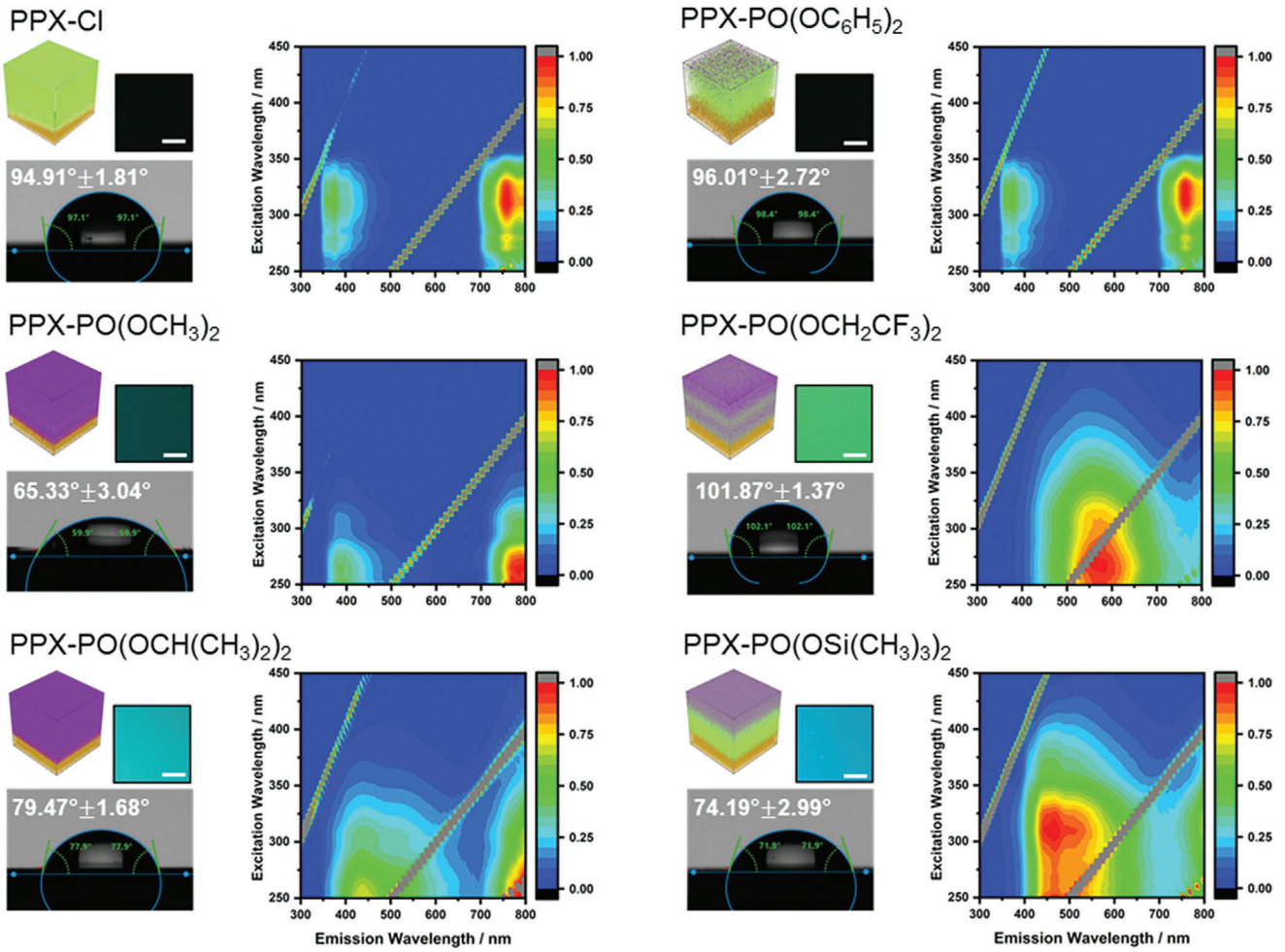

Figure 6. Surface modification by different phosphites investigated by ToF-SIMS in-depth measurements of a 500 × 500 µm sample area (*x* and *y* 500 µm, *z* not to scale), shown as a cube indicating the distribution of the fragments Cl^- (green) and PO_3^- (purple). ToF-SIMS data are combined with corresponding images of the fluorescence taken by a fluorescence microscope (scale bars represent 100 µm) and water contact angle measurements ($N = 10$) as well as the 3D fluorescence spectrum plotted as emission response to the excitation wavelengths ($\lambda_{ex} = 250$ nm to 450 nm, 5 nm increments).

transfer reaction with different phosphites of Parylene C coated silicon wafers (760 to 830 nm) for 4 h using ellipsometry and attenuated total reflectance (ATR)-IR (Supporting Information) showed the same trend in the reaction process as previously demonstrated for thin films. Here, the largest turnover of the reaction was obtained with $P(OCH_3)_3$, followed by $P(OCH(CH_3)_2)_3$ and $P(OCH_2CF_3)_3$ (Table S6 and Figure S14, Supporting Information). $P(OSi(CH_3)_3)_3$ showed evidence of the reaction, but a significant decrease in layer thickness by 194 nm (Table S6, Supporting Information) indicated that a large change in the polarity of the polymer resulted in increased chain solubility in polar solvents. This phenomenon explained the observed low fluorescence compared to the other phosphonates, as only a thin layer on the surface was functionalized. Even though only partial conversion was reached after 4 h for all surfaces and films, changes in thermal properties were detectable and in line with expectations. Due to the increase in heteroatoms, stronger electrostatic interactions occurred, resulting in higher glass transition temperatures (T_g), which were obtained for all phosphite derivatives with values in the range of 81 to 86 °C in comparison to the measured 70.4 °C for PPX-Cl (Figure 7C and Table S7, Supporting Information). Furthermore, an irregular structure and larger side groups favored lower melting temperatures for all transferred films with values of 263 to 278 °C ($T_{m;PPX\text{-}Cl}$ = 283.8 °C), as π–π stacking was hindered. Phosphonated PPX films showed a slightly increased degradation temperature $T_{95\%}$ reaching 506 °C for $PO(OCH(CH_3)_2)_2$ modification ($T_{95\%,\ PPC\text{-}Cl}$ = 477.5 °C). At the same time, thermogravimetric analysis (TGA) showed increasing residual weight (RW) at the end of the temperature ramp (approaching 1000 °C) in comparison to PPX-Cl ($RW_{PPX\text{-}Cl,\ 1000\ °C}$ = 17.1) with 25.2, 27.1, 24.96, and 29.6% for $P(OCH_3)_3$, $P(OCH(CH_3)_2)_3$, $P(OSi(CH_3)_3)_3$ and $P(OCH_2CF_3)_3$ treatment, respectively. A detailed list of the thermal properties can be found in Table S7 (Supporting Information). The demonstrated fluorescence and thermal properties of these films were comparable to the ones of phosphorous-containing

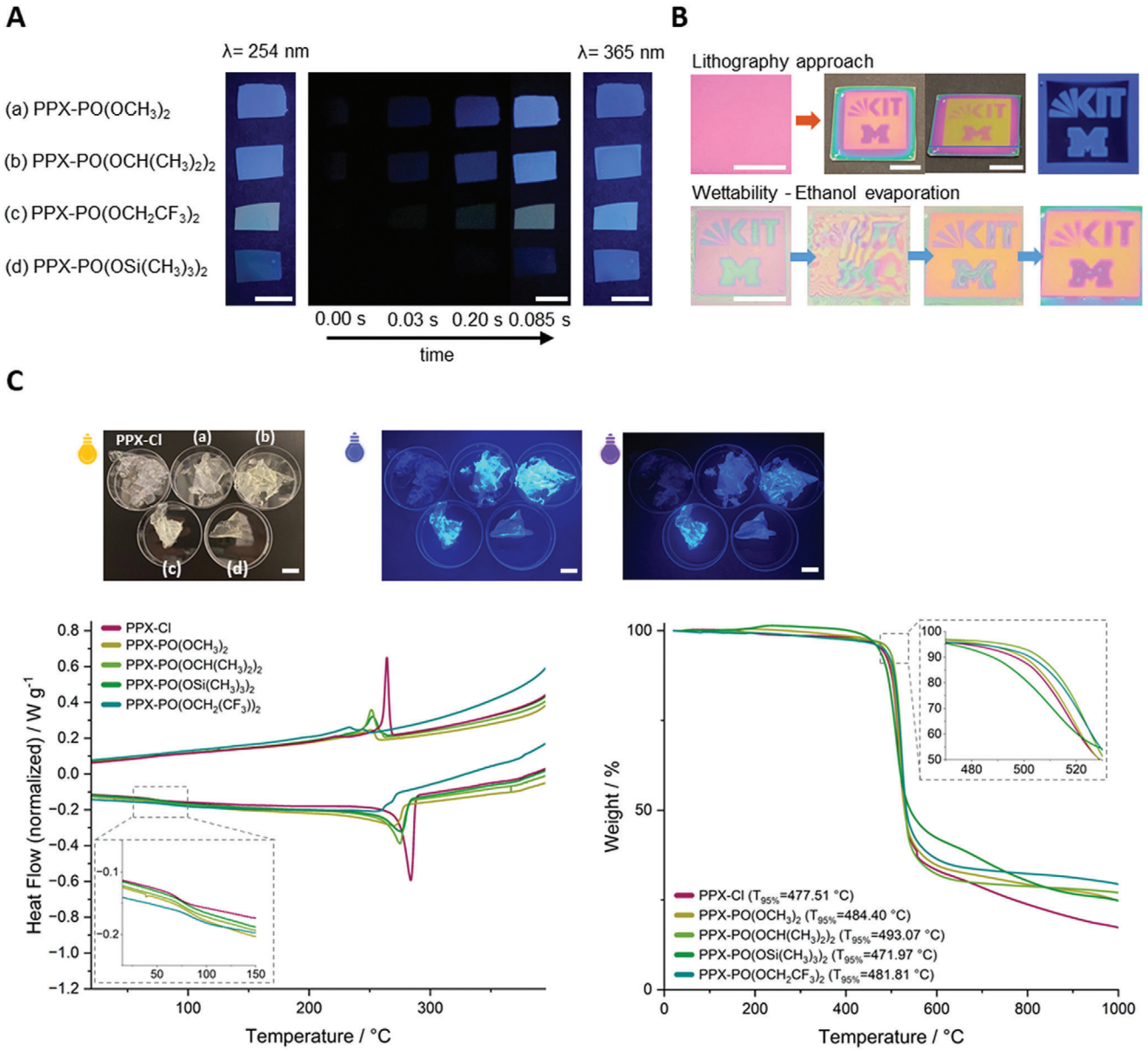

Figure 7. The properties of phosphonated PPX polymer films with thicknesses above 750 nm, indicating visible tunable fluorescence due to the choice of phosphite. The various phosphonate units also show different response times when the UV-light is switched on (A). A color change is also visible as the layer thickness increases due to the reaction. Due to the high conformality of the layer, an intrinsic angular dependence of the color can be seen. With the lithography approach, B) the evaporation of ethanol could demonstrate a different wettability. Thermal properties are demonstrated by DSC (left) and TGA (right) of transferred thin film (4 h with a) $P(OCH_3)_3$, b) $P(OCH(CH_3)_2)_3$, c) $P(OSi(CH_3)_3)_3$ and d) $P(OCH_2CF_3)_3$) with a thickness around 800 nm in addition fluorescence is demonstrated by exciting the polymer with 254 nm (violet lamp) and 365 nm (blue lamp). The scale bar indicates 1 cm.

aromatic polymers, which were recently reviewed by Ghorai and Banerjee.[47]

3. Conclusions

We developed a modular functionalization route based on commercially available Parylenes to produce phosphonated surface coatings. The CVD process is solvent-free and amenable to spatial functionalization by a photolithographic approach, leading to chemical and topographical changes whereby two tunable surface parameters are added to the functional surface. In addition, it was shown that surface properties like wettability and fluorescence were tunable through the choice of phosphite chemistry. Combining the efficient and green CVD polymerization process with a catalyst- and solvent-free transfer reaction offers a straightforward way to create new functional materials with exceptional stability and notable electronic properties. This study thus lays the groundwork for broadly applicable surface modifications with

a similar range of applications to Parylene C, but augmented by a set of additional biomimetic functions, which could be attractive for dental or orthopedic implants, bone tissue scaffolds, or integrated sensors. Phosphorous-based surface chemistry may find a broad range of applications in bioengineering, optoelectronics, energy storage, gas separation, or flame retardancy.

4. Experimental Section

Materials: All chemicals and materials were purchased from Alfa Aesar (Haverhill, MA; USA), Sigma-Aldrich (St. Louis, MO, USA), Fisher Scientific (Hampton, NH, USA), ABCR (Karlsruhe, Germany), TCI (Eschborn, Germany), SCS Germany GmbH (Pliezhausen, Germany) and used as received unless otherwise stated. Gold wafers with 100 nm thickness on 100-4 in. silicon wafers precoated with titanium for better adhesion were purchased from Georg Albert PVD-Beschichtung (Silz, Germany). Silicone wafers were obtained from Si-Mat Silicon Materials (Kaufering, Germany). The wafers were cleaned before use by washing them with acetone and ethanol and drying them under an argon stream. The custom-built chemical vapor deposition setup is from Kurt J. Lesker Company (Dresden, Germany). For the chemical transfer reaction of the PPX films, a Rayonet Photochemical Reactor 200 (RPR-200) from the Southern New England Ultraviolet Company (Branford, England) with RPR-2537A° lamps was used with a center intensity of 12.8 W cm^{-2} according to the manufacturer's specifications.

Characterization: Methods are given in the Supporting Information.

CVD Polymerization: Poly(p-xylylene) (PPX) derivatives were synthesized via a custom-built chemical vapor deposition setup following a previously reported routine, shown in Figure 1.[74] The desired amount (10, 25, 50, 750 mg) of the monomer 4,13-dichloro[2.2]paracyclophane, also known by the trade name Parylene C dimer, was sublimed under vacuum at ≈105 °C and converted into the corresponding quinodimethanes by pyrolysis in the furnace at 660 °C. Subsequently, polymerization occurs upon condensation on the substrate surface, placed on a rotating stage maintained at 15 °C in the deposition chamber. A constant deposition rate of 0.2–0.6 Å s^{-1}, determined via a deposition controller (XTC/3, Inficon GmbH, Cologne, Germany), was maintained throughout the deposition process. The rotation of the sample holder ensures a homogeneous polymer application. Argon, with a constant flow rate of 20.0 sccm, was used as a carrier gas for the CVD process, resulting in a working pressure of 0.124 mbar using an opening of the butterfly valve of the pump of 100%. The wall of the deposition chamber is heated to a constant value of 73 °C to prevent any residual deposition on the chamber walls. Finally, the coated surfaces were cleaned thrice with acetone and ethanol.

Postmodification of Parylene C with Various Phosphites: The substrate coated with Parylene C was placed in a quartz glass vessel with a lid, covered with phosphite, and treated with UV light with a wavelength of 251 nm for the desired time. To create patterned surfaces, the TEM grids were glued to the substrate at the edges with super glue and left to dry overnight, followed by the previous standard treatment. The functional surfaces were cleaned by washing them three times with acetone and ethanol. Subsequently, the substrate was immersed in ethanol for at least one hour, washed for three cycles with acetone and ethanol, and dried with argon.

Hydrolysis of Protected Phosphonated Parylene Film: The functional surfaces were treated with a mixture of conc. HCl (12 M)/water mixture (1:1%, v/v) for 2 h at 120 °C. The functional surfaces were cleaned by washing them three times with water, acetone, and ethanol. Subsequently, the substrate was immersed in water for at least one hour, washed again for three cycles with water, acetone, and ethanol, and dried with argon.

Supporting Information

Supporting Information is available from the Wiley Online Library or from the author.

Acknowledgements

The authors acknowledge funding from the Helmholtz Association program "Materials System Engineering" at the Karlsruhe Institute of Technology (KIT) and from the Deutsche Forschungsgemeinschaft (DFG) under Germany's Excellence Strategy - 3DMM2O - EXC-2082/1-390761711. The authors thank the technical and analytical staff at IFG and IBG3 (KIT). Furthermore, the authors thank Prof. Franzreb's working group for providing the 3D-printed mask.

Conflict of Interest

The authors declare no conflict of interest.

Data Availability Statement

The data that support the findings of this study are available from the corresponding author upon reasonable request.

Keywords

chemical vapor deposition (CVD) polymerization, Parylene, photolithography, postmodification

Received: February 26, 2024
Revised: April 2, 2024
Published online:

[1] M. Szwarc, *Nature* **1947**, *160*, 403.
[2] M. Szwarc, *J. Chem. Phys.* **1948**, *16*, 128.
[3] W. F. Gorham, *J. Polym. Sci., Part A-1: Polym. Chem.* **1966**, *4*, 3027.
[4] Y. L. Yeh, W. F. Gorham, *J. Org. Chem.* **1969**, *34*, 2366.
[5] F.-Y. Chou, T. C. Ramli, C.-Y. Lee, S.-M. Hu, J. Christy, H.-Y. Chen, *Org. Mater.* **2023**, *5*, 118.
[6] T. Moss, A. Greiner, *Adv. Mater. Interfaces* **2020**, *7*, 1901858.
[7] A. Kachroudi, A. Kahouli, J. Legrand, F. Jomni, *J. Phys. Chem. A* **2015**, *119*, 6428.
[8] A. Gusev, K. Mailyan, A. Pebalk, I. Ryzhikov, S. Chvalun, *J. Commun. Technol. Electron.* **2009**, *54*, 833.
[9] J.-M. Park, H. Lee, G. Lee, S. C. Jang, Y. H. Chang, H. Hong, K.-B. Chung, K. J. Lee, D. H. Kim, H.-S. Kim, *ACS Appl. Mater. Interfaces* **2022**, *15*, 1525.
[10] J. C. Salamone, *Concise Polymeric Materials Encyclopedia*, CRC Press, Boca Raton, FL **1998**.
[11] L. Jiang, G. Lu, Y. Zeng, Y. Sun, H. Kang, J. Burford, C. Gong, M. S. Humayun, Y. Chen, Q. Zhou, *Nat. Commun.* **2022**, *13*, 3853.
[12] R. Caldwell, M. G. Street, R. Sharma, P. Takmakov, B. Baker, L. Rieth, *Biomaterials* **2020**, *232*, 119731.
[13] M. Chen, H. Huang, E. Pierstorff, E. Shin, E. Robinson, D. Ho, *Ann. Biomed. Eng.* **2009**, *37*, 2003.
[14] T. Prodromakis, K. Michelakis, T. Zoumpoulidis, R. Dekker, C. Toumazou, in Sensors, 2009 IEEE, **2009**, IEEE, Christchurch, New Zealand pp. 791–794.
[15] A. Hogg, T. Aellen, S. Uhl, B. Graf, H. Keppner, Y. Tardy, J. Burger, *J. Micromech. Microeng.* **2013**, *23*, 075001.
[16] Z. You, L. Wei, M. Zhang, F. Yang, X. Wang, *IEEE Sens. J.* **2022**, *22*, 23633.
[17] B. J. Kim, E. Meng, *Polym. Adv. Technol.* **2016**, *27*, 564.
[18] H. Kim, J. Lee, B. Kim, H. R. Byun, S. H. Kim, H. M. Oh, S. Baik, M. S. Jeong, *Sci. Rep.* **2019**, *9*, 15461.

[19] H.-Y. Chen, Y. Elkasabi, J. Lahann, *J. Am. Chem. Soc.* **2006**, *128*, 374.
[20] Y. Chen, W. Pei, R. Tang, S. Chen, H. Chen, *Sens. Actuators, A* **2013**, *189*, 143.
[21] H.-Y. Chen, J. Lahann, *Langmuir* **2011**, *27*, 34.
[22] Z. Hassan, D. Varadharajan, C. Zippel, S. Begum, J. Lahann, S. Bräse, *Adv. Mater.* **2022**, *34*, 2201761.
[23] Y.-R. Chiu, Y.-T. Hsu, C.-Y. Wu, T.-H. Lin, Y.-Z. Yang, H.-Y. Chen, *Chem. Mater.* **2020**, *32*, 1120.
[24] Y.-C. Chiang, H.-W. Yeh, S.-M. Hu, C.-Y. Wu, T.-Y. Wu, C.-H. Chen, P.-C. Liao, Z.-Y. Guan, N.-C. Cheng, H.-Y. Chen, *Mater. Today Bio* **2022**, *13*, 100213.
[25] G. Duan, S. Jiang, T. Moss, S. Agarwal, A. Greiner, *Polym. Chem.* **2016**, *7*, 2759.
[26] K. C. Cheng, M. A. Bedolla-Pantoja, Y.-K. Kim, J. V. Gregory, F. Xie, A. de France, C. Hussal, K. Sun, N. L. Abbott, J. Lahann, *Science* **2018**, *362*, 804.
[27] D. Varadharajan, K. Nayani, C. Zippel, E. Spuling, K. C. Cheng, S. Sarangarajan, S. Roh, J. Kim, V. Trouillet, S. Bräse, *Adv. Mater.* **2021**, *34*, 2108386.
[28] S. Begum, F. Behboodi-Sadabad, Y. Pramudya, C. Dolle, M. Kozlowska, Z. Hassan, C. Mattern, S. Gorji, S. Heißler, A. Welle, *Chem. Mater.* **2022**, *34*, 6268.
[29] T.-H. Kim, Z. Song, J. Jung, J.-S. Sung, M.-J. Kang, W.-B. Shim, M. Lee, J.-C. Pyun, *ACS Appl. Bio Mater.* **2023**, *6*, 3726.
[30] M. Naddaka, F. Asen, S. Freza, M. Bobrowski, P. Skurski, E. Laux, J. Charmet, H. Keppner, M. Bauer, J. P. Lellouche, *J. Polym. Sci., Part A: Polym. Chem.* **2011**, *49*, 2952.
[31] T. Y. Chang, V. G. Yadav, S. De Leo, A. Mohedas, B. Rajalingam, C.-L. Chen, S. Selvarasah, M. R. Dokmeci, A. Khademhosseini, *Langmuir* **2007**, *23*, 11718.
[32] S. Gholizadeh, D. M. Lincoln, Z. Allahyari, L. P. Widom, R. N. Carter, T. R. Gaborski, *Sci. Rep.* **2023**, *13*, 4262.
[33] T. Trantidou, T. Prodromakis, C. Toumazou, *Appl. Surf. Sci.* **2012**, *261*, 43.
[34] T. Trantidou, C. Rao, H. Barrett, P. Camelliti, K. Pinto, M. Yacoub, T. Athanasiou, C. Toumazou, C. Terracciano, T. Prodromakis, *Biofabrication* **2014**, *6*, 025004.
[35] X. Deng, J. Lahann, *J. Appl. Polym. Sci.* **2014**, *131*, 40315.
[36] X. Deng, T. W. Eyster, Y. Elkasabi, J. Lahann, *Macromol. Rapid Commun.* **2012**, *33*, 640.
[37] X. Deng, J. Lahann, *Macromol. Rapid Commun.* **2012**, *33*, 1459.
[38] A.-L. Winkler, M. Koenig, A. Welle, V. Trouillet, D. Kratzer, C. Hussal, J. Lahann, C. Lee-Thedieck, *Biomacromolecules* **2017**, *18*, 3089.
[39] M. Y. Tsai, Y. C. Chen, T. J. Lin, Y. C. Hsu, C. Y. Lin, R. H. Yuan, J. Yu, M. S. Teng, M. Hirtz, M. H. C. Chen, *Adv. Funct. Mater.* **2014**, *24*, 2281.
[40] M. Herrera-Alonso, T. J. McCarthy, *Langmuir* **2004**, *20*, 9184.
[41] C. Zhang, M. E. Thompson, F. S. Markland, S. Swenson, *Acta Biomater.* **2011**, *7*, 3746.
[42] C. Satheeshkumar, B. J. Jung, H. Jang, W. Lee, M. Seo, *Macromol. Rapid Commun.* **2021**, *42*, 2000520.
[43] T. Goda, T. Konno, M. Takai, K. Ishihara, *Colloids Surf., B* **2007**, *54*, 67.
[44] D. Hao, J. Lin, R. Liu, C. Pivetti, K. Yamashiro, L. M. Schutzman, J. Sageshima, M. Kwong, N. Bahatyrevich, D. L. Farmer, *Bioact. Mater.* **2023**, *28*, 467.
[45] Z. Fohlerova, I. Gablech, A. Otahal, P. Fecko, *Adv. Mater. Interfaces* **2021**, *8*, 2001897.
[46] Q. Chen, D. Zhang, W. Zhang, H. Zhang, J. Zou, M. Chen, J. Li, Y. Yuan, R. Liu, *Nat. Commun.* **2021**, *12*, 562.
[47] A. Ghorai, S. Banerjee, *Prog. Polym. Sci.* **2023**, *138*, 101646.
[48] K. H. Lim, A. S. Lee, V. Atanasov, J. Kerres, E. J. Park, S. Adhikari, S. Maurya, L. D. Manriquez, J. Jung, C. Fujimoto, *Nat. Energy* **2022**, *7*, 248.
[49] N. Fukuda, M. Kanazawa, K. Tsuru, A. Tsuchiya, Sunarso, R. Toita, Y. Mori, Y. Nakashima, K. Ishikawa, *Sci. Rep.* **2018**, *8*, 16887.
[50] X. Cheng, X. Yang, C. Liu, Y. Li, Y. Zhang, J. Wang, X. Zhang, X. Jian, *ACS Appl. Mater. Interfaces* **2022**, *15*, 697.
[51] P. P. Tomanin, P. V. Cherepanov, Q. A. Besford, A. J. Christofferson, A. Amodio, C. F. McConville, I. Yarovsky, F. Caruso, F. Cavalieri, *ACS Appl. Mater. Interfaces* **2018**, *10*, 42786.
[52] T. Chabbah, S. Chatti, N. Jaffrezic-Renault, S. Weidner, C. Marestin, R. Mercier, *Polym. Adv. Technol.* **2023**, *34*, 2471.
[53] F. Soyekwo, C. Liu, L. Zhao, H. Wen, W. Huang, C. Cai, P. Kanagaraj, Y. Hu, *ACS Appl. Mater. Interfaces* **2019**, *11*, 30317.
[54] N. Baig, Z. Arshad, S. A. Ali, *Sci. Rep.* **2022**, *12*, 5028.
[55] S. T. Lazar, T. J. Kolibaba, J. C. Grunlan, *Nat. Rev. Mater.* **2020**, *5*, 259.
[56] F. Bahremand, T. Shahrabi, B. Ramezanzadeh, S. A. Hosseini, *Sci. Rep.* **2023**, *13*, 12169.
[57] F. Kousar, J. Malmstrom, S. Swift, J. Ross, J. Perera, S. C. Moratti, *ACS Appl. Polym. Mater.* **2021**, *3*, 2785.
[58] S. Monge, B. Canniccioni, A. Graillot, J.-J. Robin, *Biomacromolecules* **2011**, *12*, 1973.
[59] S. Hiranphinyophat, Y. Iwasaki, *Sci. Technol. Adv. Mater.* **2021**, *22*, 301.
[60] K. Ishihara, *J. Biomed. Mater. Res., Part A* **2019**, *107*, 933.
[61] R. Obrycki, C. Griffin, *Tetrahedron Lett.* **1966**, *7*, 5049.
[62] J. Plumb, R. Obrycki, C. E. Griffin, *J. Org. Chem.* **1966**, *31*, 2455.
[63] S. Oßwald, C. Zippel, Z. Hassan, M. Nieger, S. Bräse, *RSC Adv.* **2022**, *12*, 3309.
[64] Q. Dou, L. Geng, B. Cheng, C.-J. Li, H. Zeng, *Chem. Commun.* **2021**, *57*, 8429.
[65] Y. He, H. Wu, F. D. Toste, *Chem. Sci.* **2015**, *6*, 1194.
[66] R. S. Shaikh, S. J. Düsel, B. König, *ACS Catal.* **2016**, *6*, 8410.
[67] N. G. Cowper, C. P. Chernowsky, O. P. Williams, Z. K. Wickens, *J. Am. Chem. Soc.* **2020**, *142*, 2093.
[68] Y.-R. Luo, *Comprehensive Handbook of Chemical Bond Energies*, CRC Press, Boca Raton, FL **2007**.
[69] C. Galli, T. Pau, *Tetrahedron* **1998**, *54*, 2893.
[70] B. Cui, S. Jia, E. Tokunaga, N. Shibata, *Nat. Commun.* **2018**, *9*, 4393.
[71] H. F. Piedra, C. Valdés, M. Plaza, *Chem. Sci.* **2023**, *14*, 5545.
[72] K. Pruden, K. Sinclair, S. Beaudoin, *J. Polym. Sci., Part A: Polym. Chem.* **2003**, *41*, 1486.
[73] M. Bera, A. Rivaton, C. Gandon, J. Gardette, *Eur. Polym. J.* **2000**, *36*, 1765.
[74] J.-J. L. Fu, W. G. Bentrude, C. E. Griffin, *J. Am. Chem. Soc.* **1972**, *94*, 7717.
[75] S. Marque, P. Tordo, *Top. Curr. Chem.* **2005**, *250*, 43 .
[76] H. Y. Chen, J. H. Lai, X. Jiang, J. Lahann, *Adv. Mater.* **2008**, *20*, 3474.
[77] X. Zhong, R. Jordan, J.-R. Chen, J. Raymond, J. Lahann, *ACS Appl. Mater. Interfaces* **2023**, *15*, 21618.
[78] P. Jansa, O. Baszczyňski, E. Procházková, M. Dračínský, Z. Janeba, *Green Chem.* **2012**, *14*, 2282.
[79] N. Harsági, G. Keglevich, *Molecules* **2021**, *26*, 2840.
[80] R. Luschtinetz, G. Seifert, E. Jaehne, H. J. P. Adler, *Macromol. Symp.* **2007**, *254*, 248.
[81] M. J. Herman, M. W. Blair, *Polym. Degrad. Stab.* **2020**, *171*, 109024.
[82] C. N. Rusu, J. T. Yates, *J. Phys. Chem. B* **2000**, *104*, 12292.
[83] M. A. Tasdelen, Y. Yagci, *Angew. Chem., Int. Ed.* **2013**, *52*, 5930.
[84] B. D. Fairbanks, L. J. Macdougall, S. Mavila, J. Sinha, B. E. Kirkpatrick, K. S. Anseth, C. N. Bowman, *Chem. Rev.* **2021**, *121*, 6915.
[85] J. V. Jun, D. M. Chenoweth, E. J. Petersson, *Org. Biomol. Chem.* **2020**, *18*, 5747.
[86] G. Jo, Y. Park, M. H. Park, H. Hyun, *Pharmaceutics* **2023**, *15*, 1374.
[87] H. Thomas, D. L. Pastoetter, M. Gmelch, T. Achenbach, A. Schlögl, M. Louis, X. Feng, S. Reineke, *Adv. Mater.* **2020**, *32*, 2000880.
[88] D.-X. Feng, Z.-N. Gao, J. Li, Y.-H. Wang, J.-X. Hu, Z.-Z. Xue, G.-M. Wang, *Cryst. Growth Des.* **2022**, *22*, 5680.
[89] D. X. Feng, Y. Mu, J. Li, S. De Han, J. H. Li, H. L. Sun, M. Pan, J. X. Hu, G. M. Wang, *Adv. Funct. Mater.* **2023**, *33*, 2305796.